Food Chemistry: X 24 (2024) 101852

Contents lists available at ScienceDirect

Food Chemistry: X

journal homepage: www.sciencedirect.com/journal/food-chemistry-x

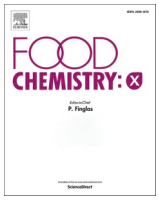

Integrated metabolomic and transcriptomic analysis revealed the transition of functional components in edible flower buds of *Hemerocallis citrina* Baroni

Congrong Jiang [a,b], Wenwen Zhang [c,b], Yating Zhang [b], Guanghui Yang [a,**], Dongmei Cao [d,**], Wei Li [a,b,c,*]

[a] College of Agriculture, Shanxi Agricultural University, Jinzhong 030801, China
[b] Shenzhen Branch, Guangdong Laboratory of Lingnan Modern Agriculture, Key Laboratory of Synthetic Biology, Ministry of Agriculture and Rural Affairs, Agricultural Genomics Institute at Shenzhen, Chinese Academy of Agricultural Sciences, Shenzhen 518120, China
[c] College of Food Science and Engineering, Shanxi Agricultural University, Jinzhong 030801, China
[d] College of Horticulture, Shanxi Agricultural University, Taiyuan 030031, China

ARTICLE INFO

Keywords:
Hemerocallis citrina Baroni
Metabolome
Edible flower buds
Flavonoids
Fatty acids

ABSTRACT

The edible flower buds of *Hemerocallis citrina* Baroni are used both as a vegetable and functional food. It has various health benefits due to the diversity of natural products. However, the establishment of functional components in the edible flower bud remains to be studied. We conducted a high-resolution metabolomic analysis of flower buds at three developmental stages, 1–2 cm, 4–6 cm, and edible (10–15 cm). Our analysis revealed 157 differential accumulated metabolites, including flavonoids (49), fatty acids (17) and terpenoids (13) while most of them decreased during flower bud development. Among them, 2 flavonoids, 2 long-chain fatty acids and 1 triterpene saponin are highly accumulated in edible flower buds. Furthermore, the expression levels of catalytic genes mirrored the changes in metabolite levels detected. These results track the dynamics of functional component accumulation during edible flower bud development, laying the theoretical basis for nutrition formation in *H. citrina*.

1. Introduction

Hemerocallis citrina Baroni, also known as Huang Hua Cai, is an important economic crop native to China, the Korean Peninsula and Japan, with flower buds used as vegetables and functional foods, as documented in the *Compendium of Materia Medica* (Li & Weng, 2020; Qing et al., 2021). *H. citrina* is known to improve sleep, calm the mind, alleviate heat and promote lactation (Du et al., 2014; Liang et al., 2021), attributed to the high content of beneficial secondary metabolites.

While metabolites vary widely across different tissues (Liu et al., 2020), changes in accumulation during different developmental stages of flower buds, particularly edible parts remain unknown. Research confirmed that the beneficial secondary metabolites in *H. citrina* are mainly flavonoids, terpenoids, phenolic acids, exhibiting various functions aside from abundant primary metabolites such as proteins, fats, sugars, vitamins, and even various essential amino acids (Liang et al., 2021; Zhao et al., 2024). The integration of metabolomics and transcriptomics analysis provides insights into the complexity and integrity of biological processes (Yang et al., 2022). Establishing a comprehensive metabolomics and transcriptomics database for *H. citrina* is imperative to document the dynamic changes in metabolite accumulation and gene expression in edible flower buds during development. Although metabolomic studies have been conducted on *H. citrina* in various parts and 144 compounds were identified (Liu et al., 2020), those parts in this study did not include bud developmental stages.

As the most important active constituents of *H. citrina*, flavonoid is a type of phenylpropanoid with a C6-C3-C6 unit and a wide range of pharmacological activities, including antiviral, antitumor, antioxidant,

* Corresponding author at: College of Agriculture, Shanxi Agricultural University, Jinzhong 030801, China; Shenzhen Branch, Guangdong Laboratory of Lingnan Modern Agriculture, Key Laboratory of Synthetic Biology, Ministry of Agriculture and Rural Affairs, Agricultural Genomics Institute at Shenzhen, Chinese Academy of Agricultural Sciences, Shenzhen 518120, China; College of Food Science and Engineering, Shanxi Agricultural University, Jinzhong, 030801, China.
** Corresponding authors.
E-mail addresses: yanggh1991@163.com (G. Yang), caodm787@163.com (D. Cao), liwei11@caas.cn (W. Li).

https://doi.org/10.1016/j.fochx.2024.101852
Received 9 July 2024; Received in revised form 18 September 2024; Accepted 20 September 2024
Available online 26 September 2024

and anti-inflammatory (Du et al., 2014; Liang et al., 2021; Lin, Chen, & Dai, 2022; Nabavi et al., 2020; Roy et al., 2022). After years of research, the flavonoid metabolic pathway shared by most plants has been well unveiled (Shen et al., 2022). The 4-coumaryl coenzyme A and malonyl-CoA are catalyzed by a series of enzymes, including chalcone synthase (CHS), chalcone reductase (CHR), chalcone isomerase (CHI), flavanone-3β-hydroxylase (F3H), flavonol synthase (FLS) and isoflavone synthase (IFS), followed by post-modification reactions such as methylation, hydroxylation, glycosylation and isoprenylation, which increased the variety of flavonoids (Lin, Chen, & Dai, 2022; Nabavi et al., 2020; Shen et al., 2022). The regulation role of numerous transcription factors (TFs) has been demonstrated for the flavonoid metabolic pathway. For instance, MBW complex for anthocyanin biosynthesis in Arabidopsis consisting of MYB113, bHLH (TT8), and the WD40 protein (TTG1), *MdWRKY11* increases flavonoids and anthocyanins accumulation in apple Calli (Gonzalez et al., 2008; Naik et al., 2022; Wang et al., 2018).

Fatty acids (FA) and triterpenoids are also important components in plant-derived food. Human requires dietary sources of fatty acid compounds with physiologically essential functions, such as linoleic acid and alpha-linolenic acid (De Carvalho & Caramujo, 2018). Fatty acids play a central role in the metabolism of living cells as building blocks of biological membranes, energy reserves of the cell, and precursors to second messenger molecules (Günenc et al., 2022). FA biosynthesis starts with acetyl-CoA and malonyl-CoA and is catalyzed by a series of fatty acid synthases localized in plastids (De Carvalho & Caramujo, 2018; Günenc et al., 2022). The following desaturation is catalyzed by fatty acid desaturases (FADs) located in the endoplasmic reticulum (He et al., 2020). Triterpenoids are a highly diverse group of natural bioactive substances widely distributed in plants (Dinday & Ghosh, 2023; Liu et al., 2024; Sawai & Saito, 2011). Triterpenoid biosynthesis involves the formation of 2,3-epoxysqualene by combining six isoprenes and then cyclized by the oxidosqualene cyclases (OSCs) into several cyclical triterpene scaffolds (Liu et al., 2024). Subsequently, Cytochrome P450s (CYPs), UDP-glycosyltransferases (UGTs), and acyltransferases (ACTs) modified these triterpene skeletons, leading to the production of a diverse array of structurally unique molecules (Dinday & Ghosh, 2023).

We employed high-resolution metabolomic analysis in different developmental stages to understand the nutrient formation in edible flower buds of *H. citrina*. The results show that the diversity of metabolites such as flavonoids, fatty acids and terpenoids decreased during maturing and 5 main specialized metabolites were retained in edible buds. The expression of catalytic and regulated genes in related biosynthesis pathways also supports the dynamic changes. Although the exact function of each compound is not known currently, this knowledge provides a valuable reference for the usage of flower buds and directs the breeding of *H. citrina* for a higher food quality.

2. Materials and methods

2.1. Plant materials

Four-year-old seedlings of the 'Meng Zi Hua' cultivar *H. citrina* (the main cultivar in the market) were grown in a greenhouse at the Shenzhen Comprehensive Experimental Base of the Chinese Academy of Agricultural Sciences (E: 114.5, N: 22.5) from 2021 to 2022. At the *H. citrina* flowering time, we randomly picked three developmental stages of flower buds: 1–2 cm flower buds, 4–6 cm flower buds, edible flower buds (specially at 15:00–16:00, 2–3 h before flowering, when the flavor is optimal) and fresh leaves of the same leaf position of corresponding plants. Three biological replicates for each parameter were set for this experiment and a total of 12 samples were obtained. For each sample, there was a mixture of at least three plants corresponding tissue to eliminate the differences between individual plants. All samples were ground to freeze-dried powder using liquid nitrogen.

2.2. Metabolite extraction

Twelve samples of 1–2 cm, 4–6 cm, edible flower buds and leaves were weighed, 0.1 g of powder was transferred to 2.0 mL centrifuge tubes, and 1.5 mL extraction solvent (methanol:water = 80:20, *v*/v) was added and mixed with a vortex for 1 min. Ultrasonic was applied then for extraction for 30 min. 1.4 mL of the supernatant was pipetted to 2.0 mL tubes after being centrifuged at 14000*g* and 4 °C for 10 min, and dried in a CV600 LABCONCO CentriVap vacuum centrifugal concentrator. Then the extracts were resuspended with 0.2 mL methanol solvent (50:50, *v*/v), and 0.1 mL were transferred to the vial for detection after centrifuged at 14000*g* and 4 °C for 20 min. A 10 μL aliquot of each sample was aspirated and mixed as a quality control sample.

2.3. Metabolomics analysis

LC-ESI-MS/MS analysis was performed with a Thermo Fisher U3000 ultra-high-performance liquid chromatography coupled with Q Exactive Plus™ Orbitrap MS system (Thermo Scientific, Waltham, MA, USA) (UHPLC-MS/MS) equipped with a heated electrospray ionization (HESI) source. The extracts were separated using a Waters ACQUITY UPLC HSS T3 C18 column (2.1 mm × 100 mm, 1.8 μm; Waters Corporation, Milford, MA, USA). The analytical column was maintained at 35 °C with an injection volume of 5 μL. Mobile phase A was acetonitrile, and solvent B was 0.1 % (*v*/v) formic acid in water. The flow rate was set as 0.2 mL/min, and the elution gradient was as follows: 0–10 min, 100 % B; 10–20 min, 100 %-70 % B; 20–25 min, 70 %-60 % B; 25–30 min, 60 %-50 % B; 30–40 min, 50 %-30 %B; 40–45 min, 30 %-0 % B; 45–60 min, 0 %B; 60–70 min, 100 % B. Both positive and negative ion modes were acquired with a range of 100–1500 *m/z*. Sheath gas flow was set as 40 arb (~ 5.35 L/min), auxiliary gas flow rate was set as 15 arb (~ 11.98 L/min), capillary temperature was set as 320 °C, and aux gas heater temperature was set as 350 °C. Positive and negative spray voltage were both set as 3.2 kv. The resolution of MS is 70,000, and the resolution of MS/MS is 17,500. Compound Discoverer 3.0 software and GNPS (https://gnps.ucsd.edu/) (Wang et al., 2016) were used for the structural identification of metabolites by comparing retention times, molecular masses, secondary fragmentation spectra and collision energies in local standard databases and other public databases such as mzVault, mzCloud and ChemSpider (shown in Figs. S9, S18 and S32). The identified metabolites were annotated and analyzed using MetaboAnalyst (https://www.metaboanalyst.ca/) and GNPS. Metabolites were quantified relatively by peak area.

2.4. Transcriptome sequencing and analysis

The same samples for metabolic analysis (≥0.1 g, $n = 3$) were sent to BGI Genomics for RNA extraction and RNA libraries were constructed for PE150 sequencing using the DIPSEQ platform. Raw data were first quality controlled using fastqc (v 0.11.9, default, https://www.bioinformatics.babraham.ac.uk/projects/fastqc/) and trim-galore (v 0.6.7, –q 30 –phred33 –length 36 –stringency 3 –paired –clip_R1 5 –clip_R2 5, https://www.bioinformatics.babraham.ac.uk/projects/trim_galore/) software. Then the clean RNA-seq reads were mapped to the *H. citrina* reference genome (Qing et al., 2021) using hisat2 software (v 2.2.1) (Kim et al., 2019), and the transcripts were assembled and quantified using stringtie software (v 2.1.7) (Pertea et al., 2015) to obtain the count and transcripts per million (TPM) data of the corresponding genes. Read mapping rates for all clean reads ranged from 87.95 % to 91.35 % (Table S4), confirming the reliability of the transcriptome data.

2.5. Difference analysis and trend clustering analysis

Difference analysis for metabolites and genes was performed using R software (v 4.3.1, https://www.R-project.org/). Differential accumulation metabolites (DAMs) were identified using fold change (FC) and

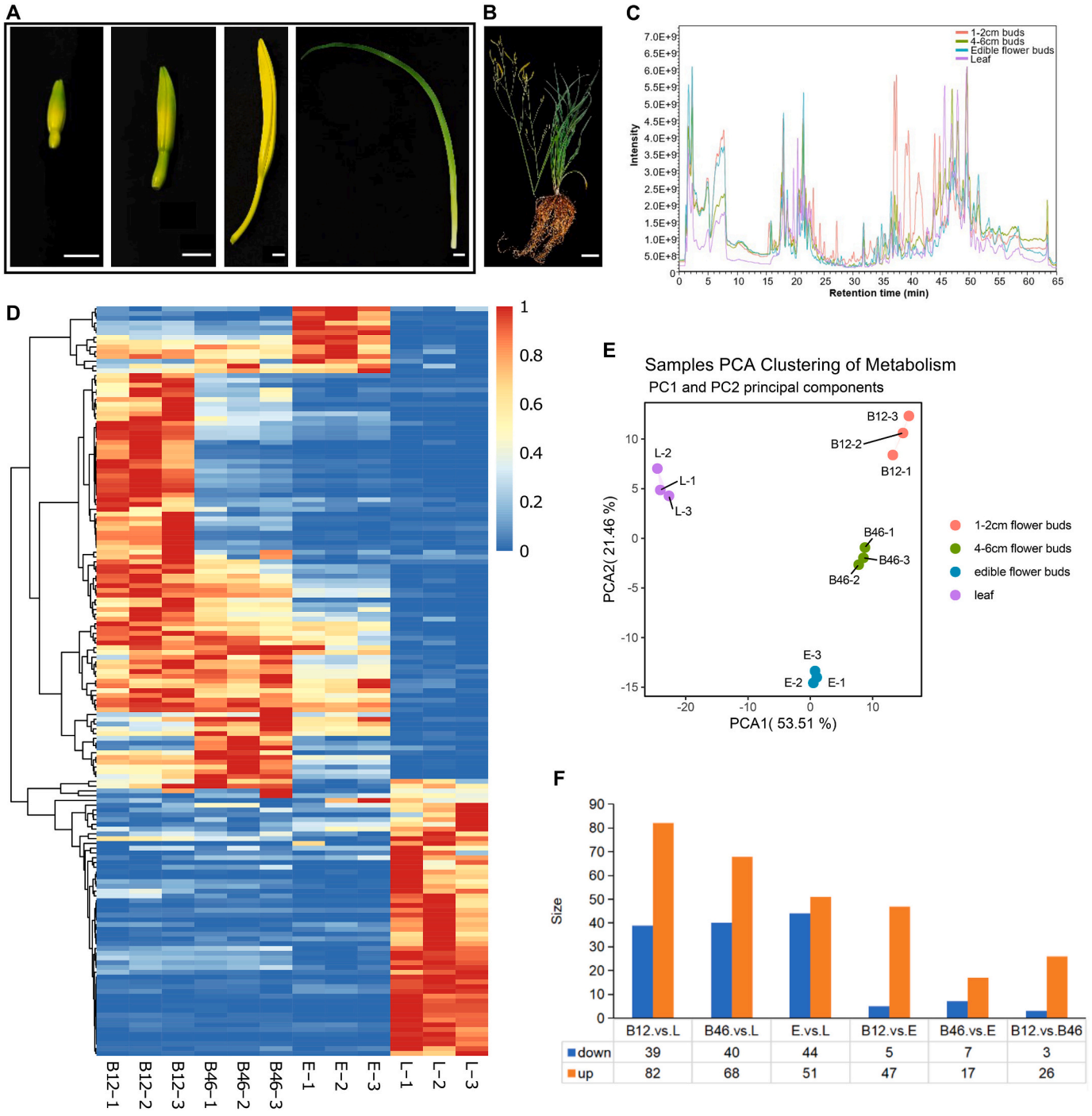

Fig. 1. Metabolome analysis for three developmental stages flower buds and leaf of *H. citrina*.
(A) Samples of three developmental stages flower and sample of leaf were collected: 1–2 cm, 4–6 cm, edible flower buds (3–5 h before flowering) and leaf. Bars in plot: 1 cm.
(B) *Hemerocallis citrina* Baroni plant. Bars in plot: 10 cm.
(C) Total ion chromatography of metabolites in four groups (positive ion modes).
(D) Clustering heatmap of the 157 DAMs. Metabolite expression values were standardised and normalised to the peak area using Linear normalisation. $|\log_2 FC| \geq 2$, p-value <0.05.
(E) PCA analysis.
(F) The number of up- and down-regulated DAMs in the different groups.
B12: 1–2 cm flower buds, B46: 4–6 cm flower buds, E: edible flower buds, L: leaf, $n = 3$.

unpaired two-tailed Student's *t*-tests ($|\log_2 FC| \geq 2$, $p < 0.05$). And identification of differentially expressed genes (DEGs) was performed with the DESeq2 package (v 1.40.2, $|\log_2 FC| \geq 1$, $p < 0.05$) (Love et al., 2014). Principal component analysis (PCA) was then performed with the FactoMineR (v 2.9) (Lê et al., 2008) and factoextra (v 1.0.7) (Alboukadel & Fabian, 2020) packages with default settings, and PCA plots, Venn diagrams, volcano plots, and others were plotted with the ggplot2 package (v 3.4.4) (Wickham, 2016). Metabolite and gene expression

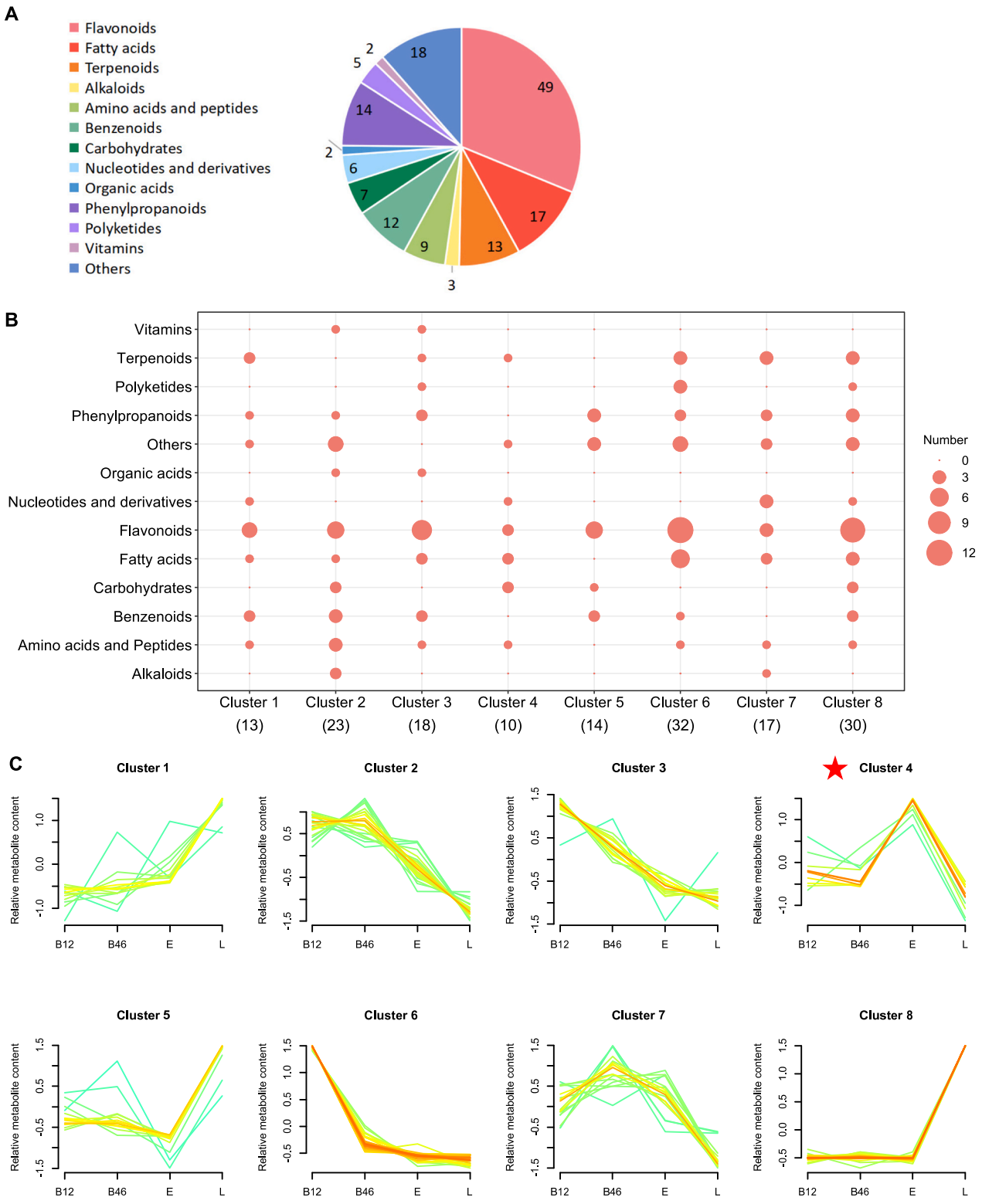

Fig. 2. Trend clustering analysis of metabolite accumulation.
(A) Group and number of 157 identified DAMs.
(B) Number of the compounds identified among different clusters. The numbers shown in each bracket (for example, 13 metabolites for Cluster 1) were derived from the number of metabolites across all 4 groups in each cluster.
(C) FCM clustering grouped the 157 identified DAMs into eight clusters.
B12: 1–2 cm buds, B46: 4–6 cm buds, E: edible flower buds, L: leaf, $n = 3$.

values were standardised and normalised by the Linear normalisation method, and heatmaps were drawn using the pheatmap package (v 1.0.12, https://cran.r-project.org/web/packages/pheatmap/index.html). Metabolite annotation and Kyoto Encyclopedia of Genes and Genomes (KEGG) pathway enrichment analysis were performed using MetaboAnalyst (https://www.metaboanalyst.ca/). Trend clustering analysis was performed according to the Fuzzy C-Means (FCM) clustering method using the Mfuzz package (v 2.60.0) (Futschik & Carlisle, 2005; Kumar & Futschik, 2007), c = 8.

2.6. Transcriptome-metabolome integration analysis

Pearson correlation analysis was performed using psych package (v 2.4.6, https://CRAN.R-project.org/package=psych). Gene function enrichment analysis was performed for the exported related module genes using R software (v 4.3.1) with the Gene Ontology (GO) and KEGG databases. The results of the analyses were plotted with the ggplot2 package (v 3.4.4) (Wickham, 2016). Pearson correlation coefficients between transcription factors (TFs) and metabolites, and between TFs and candidate genes, were calculated based on expression levels using the rcorr function of the pacman package (v 0.5.1, https://cran.r-project.org/web/packages/pacman/index.html). Network maps were generated by Cytoscape software (v 3.10.1) (Shannon et al., 2003).

2.7. Identification of genes related to metabolic pathway in H. citrina

Protein sequences of metabolic pathway-related enzymes validated in different species were downloaded from the National Center for Biotechnology Information (NCBI, https://www.ncbi.nlm.nih.gov/). Details of all downloaded genes can be found in Table S22. They were compared with the protein sequences of *H. citrina* using blastp (blast+, v 2.13.0) (Camacho et al., 2009) with an e-value ≤1e-5. Low-quality results are then filtered based on p-ident >40 % and length > 200 AA. Based on filtered *H. citrina* genes and metabolic pathway-related genes, the phylogenetic tree was constructed by Neighbor-Joining using MEGA11 software (Tamura et al., 2021) with bootstrap = 1000. Identification of metabolism pathway-related genes in *H. citrina* was based on the annotation information of these genes and whether they were located in the same branch on the phylogenetic tree as the validated metabolism pathway-related genes.

2.8. Identification of transcription factors related to metabolic pathway in H. citrina

The protein sequences of the genes were compared with the Plant Transcription Factor Database (PlantTFDB v 5.0, http://planttfdb.gao-lab.org/) to identify TFs. Pearson's correlation coefficients of TFs related to important metabolites with other key DEGs and metabolites were calculated and screened according to $|r| > 0.7$ as well as $p < 0.05$ for potential core TFs.

2.9. Validation by quantitative real-time PCR (RT-qPCR)

To validate the transcriptome sequencing data, 18 key genes were screened for RT-qPCR experiments. Total RNA of samples was extracted using FastPure® Plant Total RNA Isolation Kit (Vazyme, China). Reverse transcription of RNA was performed using the TransScript® All-in-One First-Strand cDNA Synthesis SuperMix for qPCR (TransGen, China). RT-qPCR experiments were performed on a CFX Opus 96 Real-Time PCR System (Bio-Rad, Hercules, CA, USA) using PerfectStart® Visual Green qPCR SuperMix (TransGen, China) according to the manufacturer's instructions. Relative gene expression was normalised to that of the reference gene, *60S* (*HHC040104*) (Hou et al., 2017). Gene expression levels were calculated using the $2^{-\Delta\Delta CT}$ method. All of the expression level data obtained by RT-qPCR were based on three biological replicates. Different letters indicate significant differences between different treatments according to Tukey's multiple comparisons test. Detailed primer sequences are shown in Table S23.

3. Results

3.1. Metabolic dynamics in flower bud development stages

The edible flower bud stage is the harvesting stage of *H. citrina* when the length exceeds 14 cm and the color turns completely yellow. To obtain a comprehensive understanding of the spatial and temporal variation of metabolite accumulation during flower bud development, and to explore the signature metabolites of flower bud tissue during the edible flower bud stage, three different developmental stages were collected and subjected to high-resolution metabolome analysis: 1–2 cm, 4–6 cm, edible, along with leaves (as control) (Fig. 1, Fig. S1). A total of 19,087 and 14,996 metabolic signals were detected under positive and negative ion modes, and 398 compounds were identified based on the comparison of characteristic secondary ion fragments (Fig. 1C and D, Fig. S1, Table S1). Distinct profiles were observed in the PCA analysis, whereas PCA1 and 2 captured 53.51 % and 21.46 % variance respectively (Fig. 1E).

The 398 compounds were annotated according to HMDB, PubChem, KEGG and other databases, a difference analysis was performed, and a total of 157 DAMs were identified among the four groups finally (Fig. 1, Fig. S2, Table S2). Most of the metabolites exhibited higher accumulation in 1–2 cm flower buds or leaves, and the diversity of metabolites decreased along with the flower development (Fig. 1D, Table S2). There was a total of 95 DAMs between edible flower buds and leaves, among which 51 DAMs were highly accumulated in edible flower buds. Edible flower buds revealed 5 DAMs with high accumulation and 47 DAMs with low accumulation compared with 1–2 cm flower buds, the number is 7 and 17 when compared with 4–6 cm flower buds (Fig. 1F, Fig. S2 and S3, Table S2). The diversity among the four groups suggests significant differences in the metabolic patterns during flower bud development.

Table 1
The 10 significant DAMs in Cluster 4 of metabolites.

Name	Formula	Mass error (ppm)	Theoretical *m/z* values	Experimental m/z values	RT (min)	Group
Galangin	$C_{15}H_{10}O_5$	−0.11	271.053	271.060	23.047	Flavonoids
Rutin	$C_{27}H_{30}O_{16}$	−0.97	611.153	611.160	21.405	Flavonoids
8(*S*)-hydroxy-(5Z,9E,11Z,14Z)-eicosatetraenoic acid	$C_{20}H_{32}O_3$	−1.81	319.235	319.227	33.838	Fatty acids
Linoleoyl ethanolamide	$C_{20}H_{37}NO_2$	−1.32	324.282	324.289	44.088	Fatty acids
Tetrahydrocortisone	$C_{21}H_{32}O_5$	−0.62	365.225	365.232	26.762	Terpenoids
Argininosuccinic acid	$C_{10}H_{18}N_4O_6$	−1.47	291.123	291.129	1.495	Amino acids and peptides
Galacturonic acid	$C_6H_{10}O_7$	−2.96	193.043	193.035	1.472	Carbohydrates
Uridine 5′-diphosphate	$C_9H_{14}N_2O_{12}P_2$	2.95	402.995	402.994	2.025	Carbohydrates
Uridine 5′-diphosphogalactose	$C_{15}H_{24}N_2O_{17}P_2$	−1.91	566.055	566.047	1.884	Nucleotides and derivatives
5-Methyltetrahydrofolic acid	$C_{20}H_{25}N_7O_6$	−1.27	458.187	458.179	17.235	Others

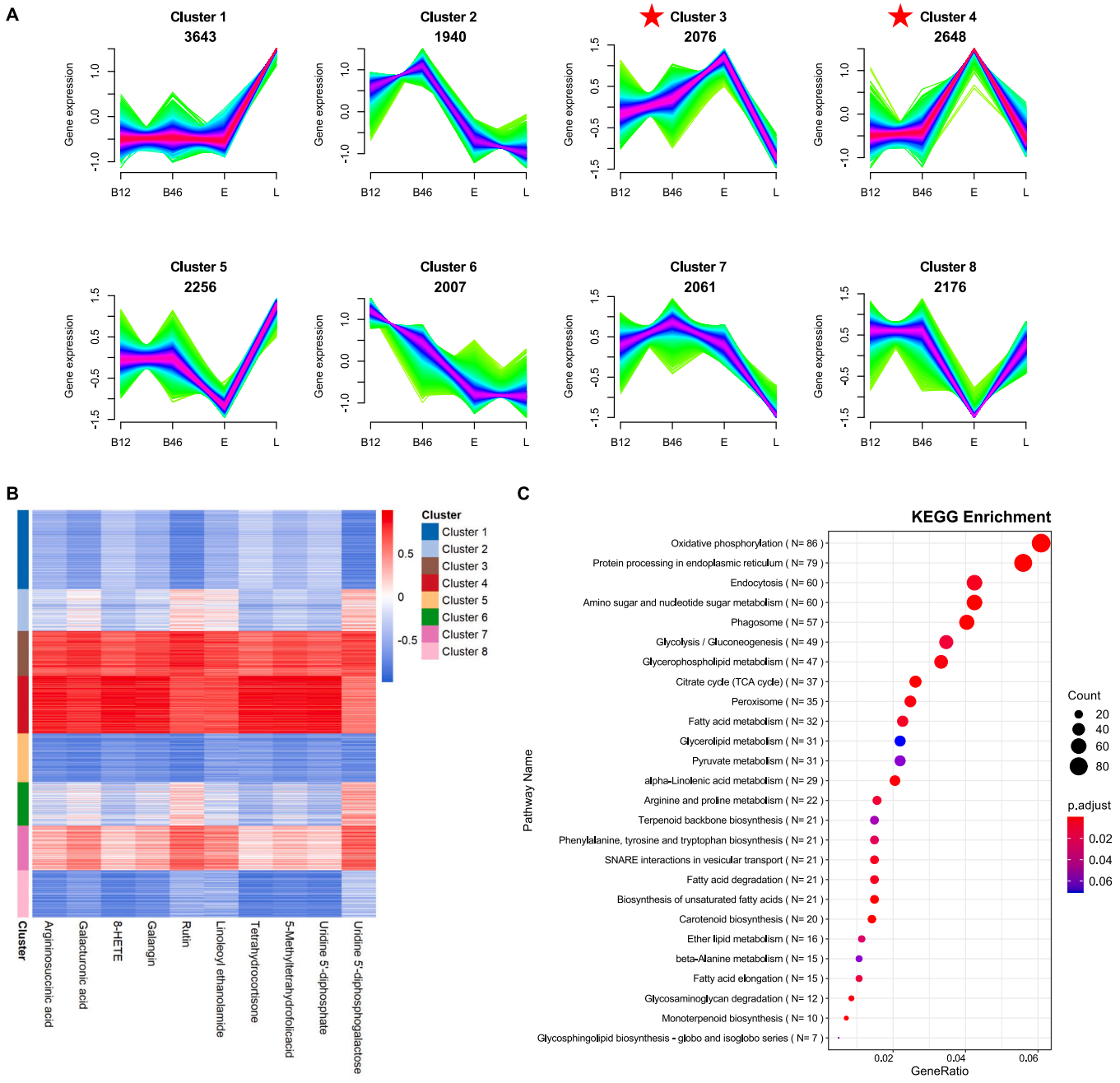

Fig. 3. Trend clustering analysis of gene expression, pearson correlation analysis and KEGG enrichment analysis of genes.
(A) FCM clustering grouped the 18,807 DEGs into eight clusters. The numbers shown in each box (for example, 3643 genes for Cluster 1) were derived from the number of genes across all 4 groups in each cluster.
(B) Correlations heatmap between gene modules and traits data on 10 DAMs highest accumulated in edible flower buds. 8-HETE, 8(*S*)-Hydroxy-(5Z,9E,11Z,14Z)-eicosatetraenoic acid.
(C) KEGG enrichment analysis of key genes. The 4308 DEGs were associated with at least 1 metabolite in Cluster 4 with $r > 0.7$ and $p < 0.05$.
B12: 1–2 cm buds, B46: 4–6 cm buds, E: edible flower buds, L: leaf, $n = 3$.

3.2. Flavonoids and fatty acids are the most varied metabolites during flower bud development

Metabolites in the flavonoid and fatty acid metabolic pathways change significantly during flower bud development. The 157 DAMs included 49 flavonoids and 17 fatty acids (Fig. 2A, Table S2). These annotated DAMs were significantly enriched in the 'Flavonoid biosynthesis', 'Flavone and flavonol biosynthesis' and 'Biosynthesis of unsaturated fatty acids' metabolic pathways according to the KEGG pathway enrichment analysis (Fig. S4, Table S3).

Using an FCM clustering algorithm, all 157 annotated metabolites were categorized into 8 clusters based on their accumulation patterns (Fig. 2B and C, Table S2). Metabolites were found to be highly accumulated significantly in 1–2 cm flower buds (Cluster 6), edible flower buds (Cluster 4), flower buds (Cluster 7), and leaves (Cluster 8), respectively. Among them, 32 metabolites from Cluster 6 were highly accumulated in 1–2 cm flower buds of *H. citrina*, and their content decreased with flower bud development, including one of the Amino

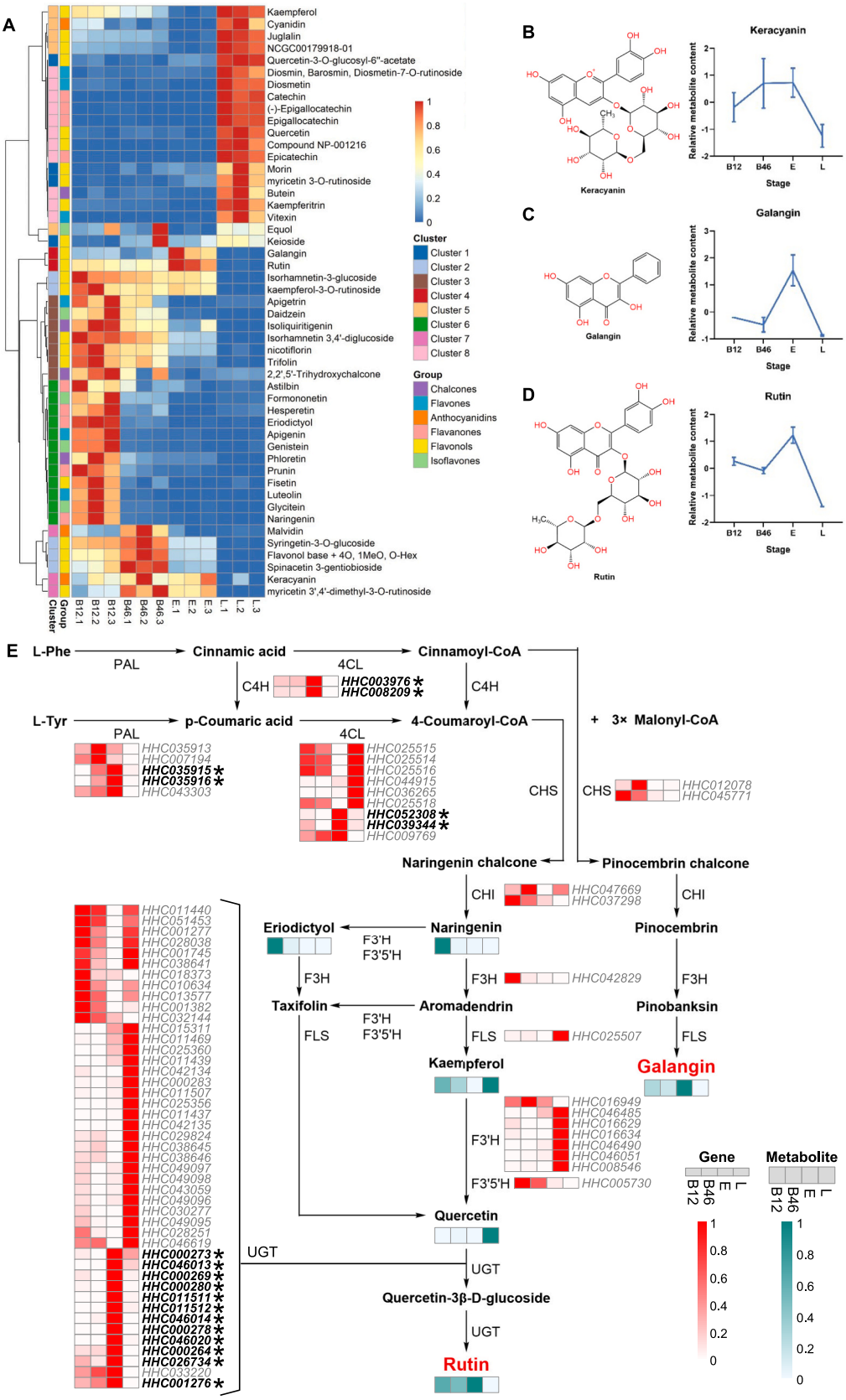

(caption on next page)

Fig. 4. Flavonoids differences analysis and metabolic pathways in *H. citrina*.
(A) Hierarchically clustered heatmap of the 49 significant DAMs of flavonoids. Metabolite expression values were standardised and normalised to the peak area using the Linear normalisation.
(B—D) Accumulation trend graphs (right) and structures (left) of Keracyanin, Galangin and Rutin.
(E) Metabolic pathways of rutin and galangin, with green boxes indicating the trend of accumulation of relevant DAMs in buds at different developmental stages and red boxes indicating the trend of expression of relevant DEGs in buds at different developmental stages. Metabolite and gene expression values were standardised and normalised to peak area and TPM using Linear normalisation. Genes marked with * indicate key genes highly associated with the characterized metabolites in the flavonoid metabolic pathway, $r > 0.7$, $p < 0.05$. PAL: Phenylalanine Ammonia-Lyase, C4H: Cinnamate 4-Hydroxylase, 4CL: 4-Coumarate: coenzyme A Ligase, CHS: Chalcone synthase, CHI: Chalcone isomerase, F3'5'H: Flavonoid-3',5'-Hydroxylase, F3'H: Flavonoid-3'-Hydroxylase, F3H: Flavanone-3β-hydroxylase, FLS: Flavonol synthase, UGT: UDP-glycosyltransferase.
B12: 1–2 cm buds, B46: 4–6 cm buds, E: edible flower buds, L: leaf, $n = 3$.

acids and peptides, twelve of Flavonoids, six of Fatty acids, three of Terpenoids, one of the Benzenoids, three of Polyketides, two of Phenylpropanoids and four of Others. Ten metabolites from Cluster 4 were highly accumulated in edible flower buds of *H. citrina*, and their content gradually increased with flower bud development, including one of Amino acids and peptides, two of Carbohydrates, two of Flavonoids, two of Fatty acids, one of Terpenoids, one of Nucleotides and derivatives and one of Others (Fig. 2B and C, Table 1, Table S2).

The most variable flavonoids during flower bud development were enriched in all eight clusters, with the highest number of types in Clusters 6 and 8 (Fig. 2B and C, Table S2 and S3). Most of the flavonoids showed the highest accumulation in 1–2 cm flower buds or leaves, except for two flavonoids in edible flower buds, and the number of flavonoid types decreased with flower bud development. Fatty acids are mainly enriched in Cluster 6 (Fig. 2B and C, Table S2). Generally, more compounds decreased the type and content during flower development and showed specificity to younger buds (Cluster 6) while just a few were enriched in edible buds.

3.3. Gene expression in flower bud stages

To understand the transcriptional regulation of metabolome during flower bud development, we conducted transcriptome sequencing on the same samples as metabolome analysis and 27,841 DEGs were identified across all groups (Fig. S5, Tables S4-S12). The number of DEGs in each group ranged from 3696 to 18,807 (Figs. S5C and S5D, Tables S7-S12). In edible flower buds, 6818 and 9968 genes were up-regulated and down-regulated compared to 1–2 cm flower buds, and 6408 and 9228 genes were up-regulated and down-regulated compared to 4–6 cm flower buds. Furthermore, edible flower buds had 9389 up-regulated and 9418 down-regulated genes compared to the leaf. There were significant differences in gene expression at different developmental stages of the flower bud, similar to the metabolome.

We utilized the same FCM method to generate 8 clusters from the expression data of a total of 18,807 flower bud development DEGs (Fig. 3A, Table S13). These results indicate that the expression trends of most genes (44.55 %) decrease with flower bud development. However, only the expression of genes in transcriptome Clusters 3 and 4 increased with flower bud development, reaching the highest levels in edible flower buds. To further validate the correlation between metabolites and genes, we calculated the Pearson correlation coefficient between them (Fig. 3B, Table S14). The 4308 DEGs in Clusters 3 and 4 were significantly and positively associated with 10 metabolites that highly accumulated in edible flower buds (Fig. 3A and B). KEGG and GO enrichment analyses showed these genes were significantly enriched in metabolic pathways related to fatty acids, such as 'Fatty acid metabolism', 'Alpha-linolenic acid metabolism', 'Biosynthesis of unsaturated fatty acids', 'Fatty acid elongation', 'fatty acid oxidation' and 'fatty acid beta-oxidation' (Fig. 3C, Fig. S6-S8, Table S15 and S16). These genes were also significantly enriched in metabolic pathways related to terpenoid, including 'Terpenoid backbone biosynthesis', 'Monoterpenoid biosynthesis', 'terpene biosynthetic process' and 'monoterpene metabolic process' (Fig. 3C, Fig. S6-S8, Table S15 and S16).

3.4. Integration analysis of flavonoid metabolism

Consequently, we first focused on the flavonoids present in *H. citrina*, and a total of 49 flavonoid DAMs were identified in our metabolic analysis (Fig. 4, Table S2). It is noteworthy that only two flavonoids, rutin and galangin, which were enriched in Cluster 4, increased during flower bud development and exhibited the highest accumulation in edible flower buds (Fig. 4A, C and D, Fig. S9, Table 1, Table S2). Keracyanin in Cluster 7 was highest accumulated in both 4–6 cm flower buds and edible flower buds (Fig. 4B, Fig. S9). However, the content of most flavonoids decreased during bud development, along with the fall of diversity. The 12 flavonoids (24.49 %) were clustered in Cluster 6, highly accumulated in the 1–2 cm flower buds, including 1 chalcone, 2 flavones, 5 flavanones, 1 flavonol and 3 isoflavones (Fig. 4A, Table S2). These are mainly flavonoid backbones and intermediates formed after a single step of hydroxylation, methylation or glycosylation, including naringenin, apigenin, eriodictyol, whose content decreases significantly with further modifications during flower bud development. In addition, 4 flavonols and 1 anthocyanidin were clustered in Clusters 2 and 7, highest accumulated in 4–6 cm flower buds, and then decreased in edible flower buds (Fig. 4A, Table S2).

The flavonoid metabolic pathway and the related genes have been widely reported (Shen et al., 2022). The structural genes and direct regulators of flavonoid metabolic pathways and the underlying themes of their regulation are highly conserved among different plant species (Gonzalez et al., 2008; Naik et al., 2022; Shen et al., 2022; Wang et al., 2018). We constructed a network map of the flavonoid metabolic pathway in *H. citrina*. Using genome annotation information and phylogenetic analysis, 75 DEGs were mapped to the flavonoid pathway (Fig. 4E, Fig. S10-S16, Table S17 and S18). During flower bud development, the expression pattern of these DEGs is identical to the accumulation pattern of their catalytic products. The up-regulation of 18 key genes (including 2 *PALs*, 2 *4CLs*, 2 *C4Hs* and 12 *UGTs*) was consistent with an increase in the content of rutin and galangin during flower bud development (Fig. 4E). The expression of other genes was almost identical to the accumulation of intermediate metabolites, being highest in 1–2 cm flower buds or 4–6 cm flower buds.

Based on the PlantTFDB database, a total of 213 TFs from 33 transcription factor families were identified to be strongly associated with increased metabolite content during flower bud development (Table S19). Correlation network maps showed that 18 flavonoid metabolic pathway-related genes and 18 TFs were strongly associated with the increase in rutin and galangin content during flower bud development (Fig. 4E, Fig. S17, Table S20 and S21).

3.5. Fatty acid and triterpenoid accumulation in edible flower bud

Subsequently, we focused on fatty acids in *H. citrina* and identified 17 fatty acid DAMs in metabolic analysis (Fig. 5). Two fatty acids, 8(*S*)-Hydroxy-(5Z,9E,11Z,14Z)-eicosatetraenoic acid and linoleoyl ethanolamide, which were enriched in Cluster 4, showed a gradual increase in content during flower bud development of *H. citrina* (Fig. 5A, B, and C, Fig. S18, Table 1, Table S2). In addition, most of the fatty acids (35.29 %) were enriched in Cluster 6, and significantly accumulated in 1–2 cm

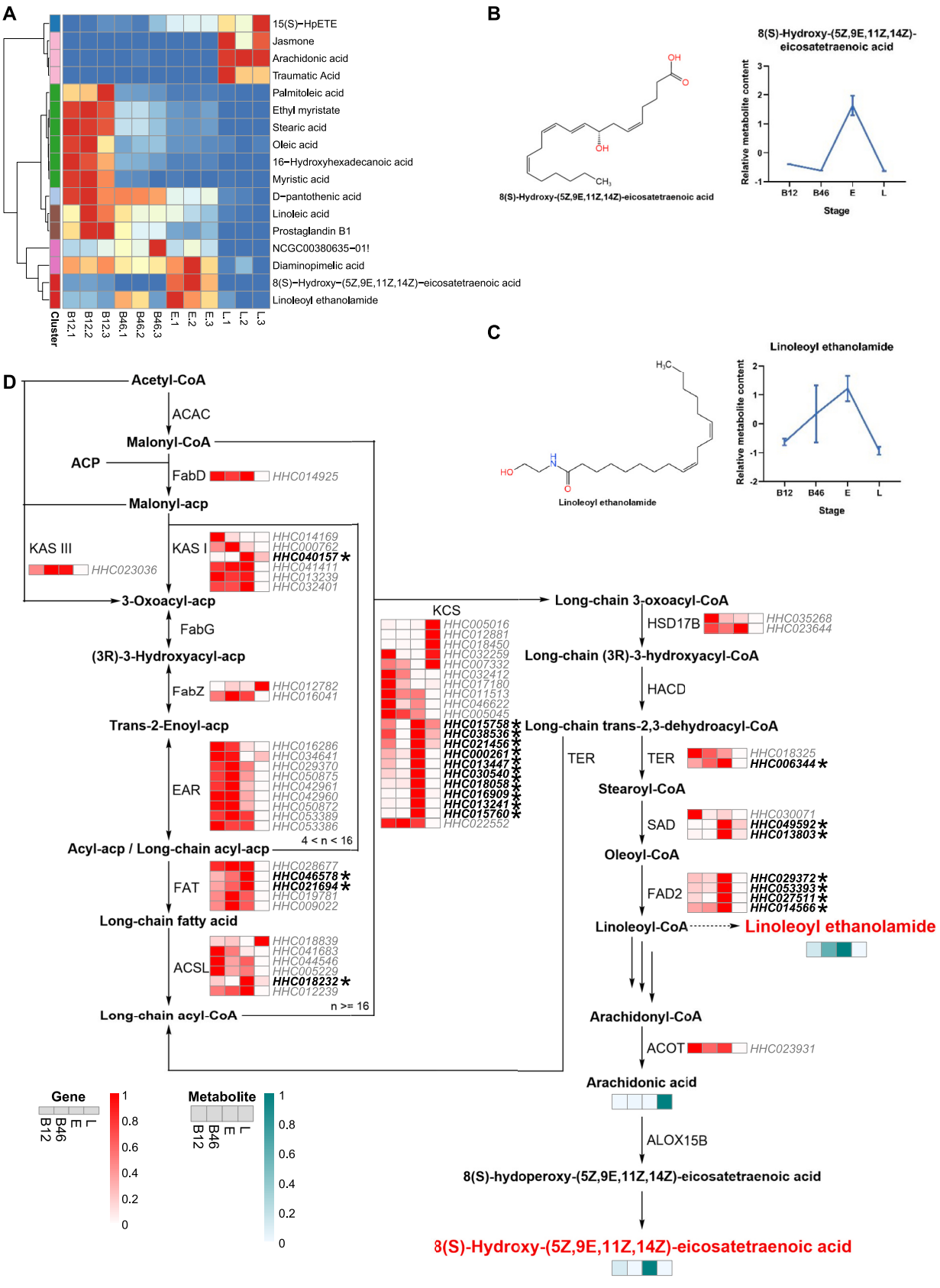

(caption on next page)

Fig. 5. Fatty acids differences analysis and metabolic pathways in *H. citrina*.
(A) Hierarchically clustered heatmap of the 17 significant DAMs of fatty acids. Metabolite expression values were standardised and normalised to peak area using the Linear normalisation.
(B—C) Accumulation trend graphs (right) and structures (left) of 8(*S*)-Hydroxy-(5Z,9E,11Z,14Z)-eicosatetraenoic acid and Linoleoyl ethanolamide.
(D) Metabolic pathways of 8(*S*)-Hydroxy-(5Z,9E,11Z,14Z)-eicosatetraenoic acid and linoleoyl ethanolamide, with green boxes indicating the trend of accumulation of relevant DAMs in buds at different developmental stages and red boxes indicating the trend of expression of relevant DEGs in buds at different developmental stages. Metabolite and gene expression values were standardised and normalised to peak area and TPM using the Linear normalisation. Genes marked with * indicate key genes highly associated with the characterized metabolites in the fatty acid metabolic pathway, $r > 0.7$, $p < 0.05$. ACAC: acetyl-CoA carboxylase, FabD: [acyl-carrier-protein] S-malonyltransferase, KAS I: 3-oxoacyl-[acyl-carrier-protein] synthase I, KAS III: 3-oxoacyl-[acyl-carrier-protein] synthase III, FabG: 3-oxoacyl-[acyl-carrier protein] reductase, FabZ: 3-hydroxyacyl-[acyl-carrier protein] dehydratase, EAR: enoyl-[acyl-carrier protein] reductase, FAT: fatty acyl-ACP thioesterase, ACSL: long-chain acyl-CoA synthetase, KCS: 3-ketoacyl-CoA synthase, HSD17B: very-long-chain 3-oxoacyl-CoA reductase, HACD: very-long-chain (3*R*)-3-hydroxyacyl-CoA dehydratase, TER: very-long-chain enoyl-CoA reductase, SAD: stearoyl-CoA desaturase, FAD2: omega-6 fatty acid desaturase, ACOT: acyl-coenzyme A thioesterase, ALOX15B: arachidonate 15-lipoxygenase B.
B12: 1–2 cm buds, B46: 4–6 cm buds, E: edible flower buds, L: leaf, $n = 3$.

flower buds, including a range of long-chain fatty acids such as Oleic acid, Myristic acid, and Stearic acid (Fig. 5A, Table S2). Fatty acid metabolic pathways and their associated genes are also well-defined (De Carvalho & Caramujo, 2018; Günenc et al., 2022; He et al., 2020). Using genome annotation information and phylogenetic analyses, 63 DEGs were mapped to fatty acid metabolic pathways (Fig. 5D, Fig. S19-S31, Table S17 and S18). The up-regulation of 21 key genes (including 1 *KAS I*, 2 *FAT*s, 1 *ACSL*, 10 *KCS*s, 1 *TER*, 2 *SAD*s and 4 *FAD2*s) was consistent with the increase in 8(*S*)-Hydroxy-(5Z,9E,11Z,14Z)-eicosatetraenoic acid and linoleoyl ethanolamide content during flower bud development in *H. citrina* (Fig. 5D).

In addition, 13 terpenoid DAMs were identified and further analyzed. The results showed that only the content of tetrahydrocortisone, which belongs to Cluster 4, gradually increased during flower bud development of *H. citrina* (Fig. 6A and B, Fig. S32, Table 1, Table S2). Three terpenoids (23.08 %) were enriched in Cluster 6, and their contents gradually decreased with flower bud development of *H. citrina*, being highest in 1–2 cm flower buds. Three terpenoids were enriched in Cluster 7, with the highest contents in 4–6 cm flower buds. The 42 DEGs were mapped to known terpenoid metabolic pathways (Fig. 6C, Fig. S33-S49, Table S17 and S18). The up-regulation of 9 key genes (including 1 *DXS*, 1 *DXR*, 3 *HDS*s, 1 *HDR*, 1 *HMGR*, 3 *GPS*s and 1 *FPS*) was consistent with an increase in tetrahydrocortisone content (Fig. 6C).

To confirm the accuracy and reproducibility of the transcriptome analysis results, 5 flavonoid genes, 8 fatty acid genes and 5 terpenoid genes were randomly selected and confirmed by RT-qPCR. For all 18 key genes, RT-qPCR analysis revealed the same expression trends as the RNA-Seq data (Fig. S50). These results confirmed the reliability of the RNA-Seq data.

4. Discussion

Plant flowers can be consumed as healthy foods in many Asian and European regions (Skrajda-Brdak et al., 2020). More than 50 edible flower foods have been recorded as local cuisines, e.g. stigmas from saffron, a precious spice in meditation regions and a valuable healthy beverage and medicine in China, rose and sweet osmanthus is used for making cakes and sauces in China, ancient Chinese were used to eat Chrysanthemums to keeping healthy (Skrajda-Brdak et al., 2020). *H. citrina* is one of the edible flowers widely used in China, fresh flower buds can be boiled or steamed for making salad and dry flowers for easier storage are used for making soups, stew and stir-fries (Du et al., 2014; Li & Weng, 2020; Liang et al., 2021; Liu et al., 2020; Qing et al., 2021; Zhao et al., 2024). Tissue-specific accumulation of beneficial ingredients in flowers allow edible flower to be not only a delicious food material but a functional food for healthy propose.

In this study, we used nontargeted metabolomic analysis based on high-resolution UHPLC-MS/MS to annotate metabolites for three developmental stages of flower bud and one leaf sample in *H. citrina*. Although 398 compounds were identified using the characteristic secondary ion fragmentation information base, there are still many metabolites represented by metabolic signals that are unknown (Fig. 1, Fig. S1, Table S1). With further improvement of the nontargeted metabolomics database, there is scope for further mining of our data.

We identified 157 annotated DAMs of various types during flower bud development in *H. citrina* (Fig. 2A and B, Table S2). The 10 metabolites in Cluster 4 displayed an increase with flower bud development and accumulated most significantly in edible flower buds (Fig. 2B and C, Table 1, Table S2). Previous studies have purified and identified more than 100 compounds from different tissues of *H. citrina*, including anthraquinones, flavonols, polyphenols and other compounds (Du et al., 2014; Liang et al., 2021; Roy et al., 2022; Zhao et al., 2024). However, more in-depth investigation into how functional components accumulate and change during the development of edible flower buds in *H. citrina*, has been lacking. This study preliminarily reveals the accumulation characteristics of various functional components in *H. citrina*. In contrast to previous studies, we found that nutrients were actually more abundant in 1–2 cm flower buds than in edible flower buds (Cluster 6), and that their diversity and content decreased with bud development (Fig. 2B and C, Table S2). It is suggested the young buds with higher nutrient diversity may be a better option for functional food compared to edible stage that used nowadays, although the biomass is less.

We found that metabolites in the flavonoid and fatty acid metabolic pathways were significantly changed during flower bud development in *H. citrina* (Fig. S4). In this study, 49 flavonoids, 17 fatty acids and 13 terpenoids changed significantly during flower bud development (Figs. 4A, 5A and 6A). The content of rutin, galangin, 8(*S*)-Hydroxy-(5Z,9E,11Z,14Z)-eicosatetraenoic acid, linoleoyl ethanolamide and tetrahydrocortisone increases with flower bud development and accumulates to a specific high level in edible flower buds (Figs. 4–6, Table 1, Table S3 and S6).

Rutin is widely distributed in fruits, vegetables, and many functional foods. Buckwheat is considered a major source, but citrus fruits, apples and tea (*Camellia sinesis*) are also known to be rich sources of rutin (Farha et al., 2022). It's a promising natural dietary supplement for the prevention and treatment of certain cancers (Farha et al., 2022). In *H. citrina*, rutin is specifically accumulated in edible flower buds that may related to the function of anti-tumour (Farha et al., 2022), antidepressant (Du et al., 2014) and sleep-improvement (Liang et al., 2021). Galangin can be found in honey, propolis, *Alpinia officinarum*, and *Helichrysum aureonitens* (Thapa et al., *2023*). As an inflammation modulator and a powerful free radical scavenger, galangin may enhance the immune response and prevent several diseases, including neurological, cardiovascular, skin, liver and kidney diseases (Thapa et al., 2023). In *H. citrina*, galangin is also specifically accumulated in edible flower buds and may related to the function of anti-inflammatory, antioxidant, hepatoprotective and cardioprotective. As a nutrient, Linoleoyl ethanolamide is present in cereals (especially wheat-based foods), coffee powder, cocoa, carrots, margarine, eggs, and legumes (Tovar et al., 2023). Linoleoyl ethanolamide is one of the bioactive lipids derived

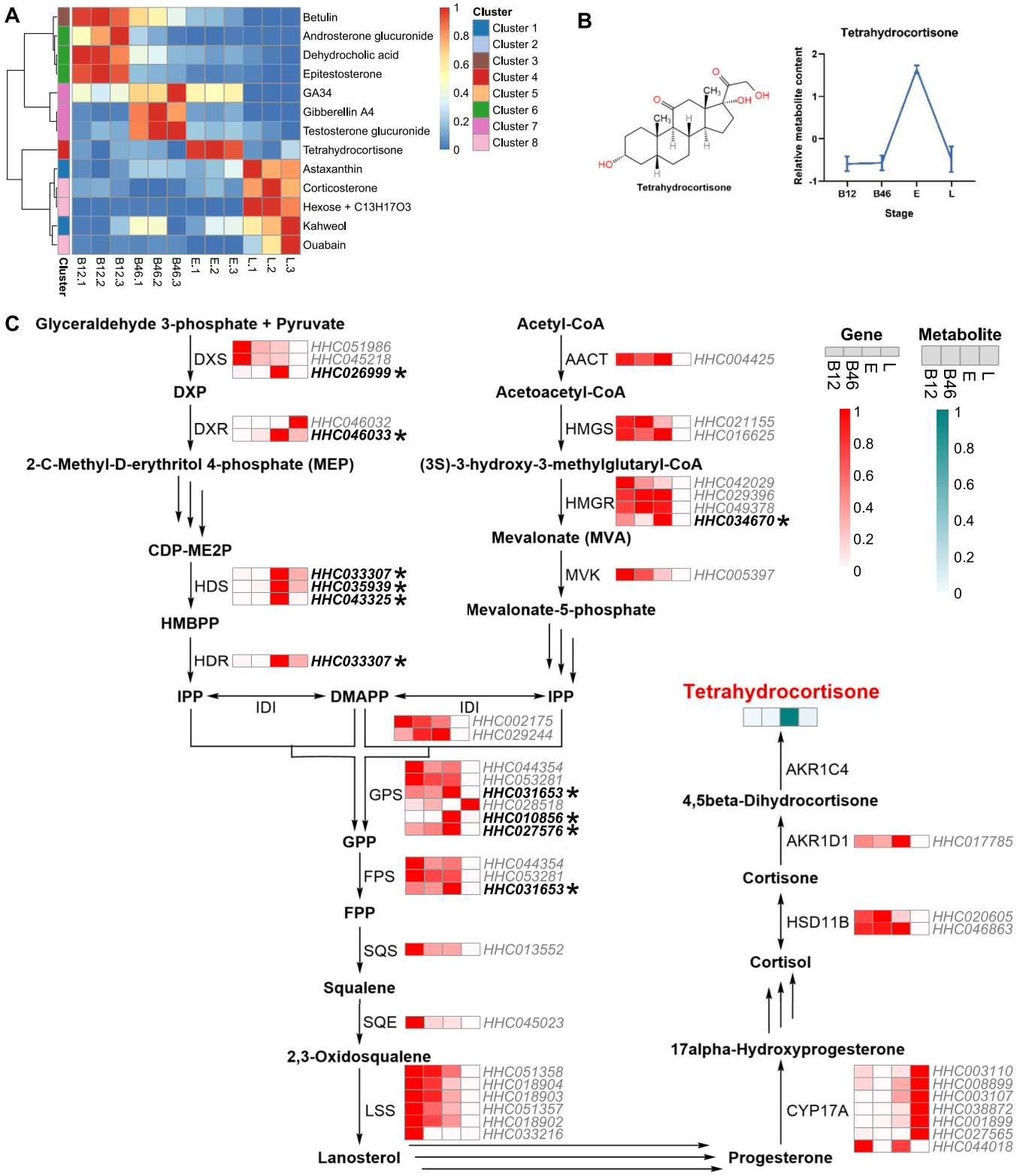

(caption on next page)

Fig. 6. Terpenoids differences analysis and metabolic pathways in *H. citrina*.
(A) Hierarchically clustered heatmap of the 13 significant DAMs of terpenoids. Metabolite expression values were standardised and normalised to peak area using the Linear normalisation.
(B) Accumulation trend graphs (right) and structures (left) of Tetrahydrocortisone.
(C) Metabolic pathways of tetrahydrocortisone, with green boxes indicating the trend of accumulation of relevant DAMs in buds at different developmental stages and red boxes indicating the trend of expression of relevant DEGs in buds at different developmental stages. Metabolite and gene expression values were standardised and normalised to peak area and TPM using the Linear normalisation. Genes marked with * indicate key genes highly associated with the characterized metabolites in the terpenoid metabolic pathway, $r > 0.7$, $p < 0.05$. DXS: 1-deoxy-D-xylulose-5-phosphate synthase, DXR: 1-deoxy-D-xylulose-5-phosphate reductoisomerase, HDS: 4-hydroxy-3-methylbut-2-enyl diphosphate synthase, HDR: 4-hydroxy-3-methylbut-2-enyl diphosphate reductase, AACT: acetyl-CoA *C*-acetyltransferase, HMGS: hydroxymethylglutaryl-CoA synthase, HMGR: hydroxymethylglutaryl-CoA reductase, MVK: mevalonate kinase, IDI: isopentenyl-diphosphate Delta-isomerase, GPS: geranyl diphosphate synthase, FPS: farnesyl diphosphate synthase, SQS: Squalene synthase, SQE: Squalene monooxygenase, LSS: lanosterol synthase, CYP17A: steroid 17alpha-monooxygenase, HSD11B: corticosteroid 11-beta-dehydrogenase isozyme, AKR1D1: 3-oxo-5-beta-steroid 4-dehydrogenase, AKR1C4: 3alpha-hydroxysteroid 3-dehydrogenase / chlordecone reductase.
B12: 1–2 cm buds, B46: 4–6 cm buds, E: edible flower buds, L: leaf, $n = 3$.

from dietary fatty acids that modulate important homeostatic functions, including appetite, fatty acid synthesis, mitochondrial respiration, inflammation, and nociception, and may also be used as a nutritional supplement or modulator (Tovar et al., 2023). The function of these highly accumulated metabolites may explain the reason for the anti-inflammatory and analgesic effects of the edible flower buds of *H. citrina*.

At present, few literatures have studied the fatty acids and terpenoids from edible flowers of *H. citrina* in detail. Compared to previous research (Du et al., 2014; Zhao et al., 2024), we identified a greater variety of differential flavonoids, fatty acids and terpenoids during flower bud development and showed for the first time that besides rutin, the galangin, 8(*S*)-Hydroxy-(5Z,9E,11Z,14Z)-eicosatetraenoic acid, linoleoyl ethanolamide and tetrahydrocortisone also accumulate specifically in edible flower buds of *H. citrina* (Figs. 4–6). Furthermore, the functional component content of Cluster 7 was essentially unchanged for the same weight of flower buds (Fig. 2B). However, as the weight of the flower buds increased during development, the total amount of these functional components may have increased significantly, and this was reflected at another level as a significant accumulation in the edible flower buds. These components include keracyanin, diaminopimelic acid, citric acid, and 6-methylquinoline, and merit further investigation.

The 4308 DEGs were up-regulated during flower bud development in *H. citrina* (Fig. 3A, Fig. S4, Tables S4-S13), corresponding to the 10 metabolites. Transcriptional regulation and gene expression exhibit similar developmental control expression patterns as metabolite accumulation (Yang et al., 2022). Previous transcriptomic studies have only identified 7395 DEGs associated with flower development (Yang et al., 2020) and established 43 EST-SSR markers for varietal identification (Li & Weng, 2020) in *H. citrina*. However, their data lack support of the reference genome, potentially resulting in incomplete gene assembly and a higher probability of assembly error, and none of these studies investigated the associated metabolic pathways. We further validated the strong positive correlation between these genes and increased metabolite content by Pearson correlation analysis (Fig. 3B, Tables S14-S16). In the KEGG and GO enrichment analysis, it is evident that genes are significantly enriched in metabolic pathways of fatty acid and terpenoid (Fig. 3C, Figs. S6-S8, Table S15 and S16).

A comprehensive network diagram of metabolic pathways during flower bud development in *H. citrina* showed that the 18 up-regulated key genes and 18 TFs were strongly correlated with the increased content of rutin and galangin (Fig. 4E, Fig. S17, Tables S17-S21). The up-regulation of 21 key genes was consistent with the increase in 8(*S*)-Hydroxy-(5Z,9E,11Z,14Z)-eicosatetraenoic acid and linoleoyl ethanolamide content (Fig. 5D, Table S17 and S18). The up-regulation of 9 key genes was consistent with an increase in tetrahydrocortisone content (Fig. 6C, Table S17 and S18). These genes may be involved in metabolic pathways of flavonoid, fatty acid and terpenoid, the specific functions of which need to be further validated. We used RT-qPCR experiments to show that the expression trends of these key genes were consistent with the RNA-seq data (Fig. S50, Table S23). There are few reports on the synthesis and regulation of bioactive metabolites in *H. citrina*. A previous study has predicted some candidate genes for rutin biosynthesis in *H. citrina* based on differences between different tissues (Qing et al., 2021). Our results not only encompass the candidate genes previously reported by Qing (Qing et al., 2021) but also offer insights into flower buds at different developmental stages, providing novel perspectives on the accumulation and regulation of bioactive metabolites in *H. citrina* flower buds.

5. Conclusion

In conclusion, this study measured and co-analyzed the high-resolution metabolome and transcriptome of *H. citrina* flower buds at different developmental stages, and elucidated the dynamics of functional component accumulation during the development of the most important tissue, the edible flower buds, in *H. citrina*. The expression levels of catalytic genes as well as transcription factors associated with flavonoid, fatty acid and terpenoid metabolic pathways mirrored the changes in metabolite levels detected during flower buds development.

H. citrina is a perennial plant with a complex genetic background and an extended growth cycle of at least 4–5 years to achieve a stable yield. This limitation has significantly hindered the development of the *H. citrina* industry in China (Li & Weng, 2020; Qing et al., 2021). This study serves as a theoretical reference for the multi-omics-assisted selection of traits with excellent characteristics and stable quality but also contributes to the exploration of metabolic pathway for functional components in *H. citrina*. It establishes a foundation and reference for further research on the mechanism of nutrition formation in *H. citrina*.

Funding

Agricultural Science and Technology Innovation Project of Shanxi Agricultural University (YGC20203).

National Key Research and Development Program of China (Grant No. 2020YFA0907900).

CRediT authorship contribution statement

Congrong Jiang: Writing – original draft, Visualization, Investigation, Data curation, Conceptualization. **Wenwen Zhang:** Writing – review & editing, Investigation. **Yating Zhang:** Writing – review & editing, Supervision, Methodology. **Guanghui Yang:** Writing – review & editing, Supervision. **Dongmei Cao:** Writing – review & editing, Supervision, Resources, Funding acquisition. **Wei Li:** Writing – review & editing, Supervision, Resources, Funding acquisition, Conceptualization.

Declaration of competing interest

The authors declare that they have no known competing financial interests or personal relationships that could have appeared to influence the work reported in this paper.

Data availability

Data will be made available on request. The transcriptome data in this study were submitted to the NCBI (https://www.ncbi.nlm.nih.gov/) under the bioproject accession PRJNA1131082.

Acknowledgment

We thank Dr. Ran Du from Agricultural Genomics Institute at Shenzhen, Chinese Academy of Agricultural Sciences for guidance of metabolome analysis; we wish to thank BGI Genomics for transcriptome sequencing support.

Appendix A. Supplementary data

Supplementary data to this article can be found online at https://doi.org/10.1016/j.fochx.2024.101852.

References

Alboukadel, K., & Fabian, M. (2020). Extract and visualize the results of multivariate data analyses [R package factoextra version 1.0.7]. Semantic Scholar. https://www.semanticscholar.org/paper/Extract-and-Visualize-the-Results-of-Multivariate-Kassambara-Mundt/5cb503e3db8609405d9f286fadc2a8bb867e5b6e.

Camacho, C., Coulouris, G., Avagyan, V., Ma, N., Papadopoulos, J., Bealer, K., et al. (2009). BLAST+: Architecture and applications. *BMC Bioinformatics, 10*(1), 421.

De Carvalho, C. C. C. R., & Caramujo, M. J. (2018). The various roles of fatty acids. *Molecules, 23*(10), 2583.

Dinday, S., & Ghosh, S. (2023). Recent advances in triterpenoid pathway elucidation and engineering. *Biotechnology Advances, 68*, Article 108214.

Du, B., Tang, X., Liu, F., Zhang, C., Zhao, G., Ren, F., et al. (2014). Antidepressant-like effects of the hydroalcoholic extracts of *Hemerocallis citrina* and its potential active components. *BMC Complementary and Alternative Medicine, 14*(1), 326.

Farha, A. K., Gan, R. Y., Li, H. B., Wu, D. T., Atanasov, A. G., Gul, K., et al. (2022). The anticancer potential of the dietary polyphenol rutin: Current status, challenges, and perspectives. *Critical Reviews in Food Science and Nutrition, 62*(3), 832–859.

Futschik, M. E., & Carlisle, B. (2005). Noise-robust soft clustering of gene expression time-course data. *Journal of Bioinformatics and Computational Biology, 03*(04), 965–988.

Gonzalez, A., Zhao, M., Leavitt, J. M., & Lloyd, A. M. (2008). Regulation of the anthocyanin biosynthetic pathway by the TTG1/bHLH/Myb transcriptional complex in arabidopsis seedlings. *The Plant Journal, 53*(5), 814–827.

Günenc, A. N., Graf, B., Stark, H., & Chari, A. (2022). Fatty acid synthase: Structure, function, and regulation. *Macromolecular Protein Complexes IV: Structure and Function, 99*, 1–33.

He, M., Qin, C. X., Wang, X., & Ding, N. Z. (2020). Plant unsaturated fatty acids: Biosynthesis and regulation. *Frontiers in Plant Science, 11*, 390.

Hou, F., Li, S., Wang, J., Kang, X., Weng, Y., & Xing, G. (2017). Identification and validation of reference genes for quantitative real-time PCR studies in long yellow daylily, *Hemerocallis citrina* Borani. *PLoS One, 12*(3), Article e0174933.

Kim, D., Paggi, J. M., Park, C., Bennett, C., & Salzberg, S. L. (2019). Graph-based genome alignment and genotyping with HISAT2 and HISAT-genotype. *Nature Biotechnology, 37*(8), 907–915.

Kumar, L. E., & Futschik, M. (2007). Mfuzz: A software package for soft clustering of microarray data. *Bioinformation, 2*(1), 5–7.

Lê, S., Josse, J., & Husson, F. (2008). FactoMineR: An R package for multivariate analysis. *Journal of Statistical Software, 25*, 1–18.

Li, S., & Weng, Y. (2020). Characterization of *Hemerocallis citrina* transcriptome and development of EST-SSR markers for evaluation of genetic diversity and population structure of *Hemerocallis* collection. *Frontiers in Plant Science, 11*, 686.

Liang, Y., Huang, R., Chen, Y., Zhong, J., Deng, J., Wang, Z., et al. (2021). Study on the sleep-improvement effects of *Hemerocallis citrina* Baroni in *Drosophila melanogaster* and targeted screening to identify its active components and mechanism. *Foods, 10*(4), 883.

Lin, C., Chen, D., & Dai, J. (2022). Advances of synthetic biology of flavonoids. *Acta Pharmaceutica Sinica, 57*(5), 1322–1335.

Liu, J., Yin, X., Kou, C., Thimmappa, R., Hua, X., & Xue, Z. (2024). Classification, biosynthesis, and biological functions of triterpene esters in plants. *Plant Communications, 5*(4), Article 100845.

Liu, J., Zhong, X., Jiang, Y., Yu, L., Huang, X., Dong, Z., et al. (2020). Systematic identification metabolites of *Hemerocallis citrina* borani by high-performance liquid chromatography/quadrupole-time-of-flight mass spectrometry combined with a screening method. *Journal of Pharmaceutical and Biomedical Analysis, 186*, Article 113314.

Love, M. I., Huber, W., & Anders, S. (2014). Moderated estimation of fold change and dispersion for RNA-seq data with DESeq2. *Genome Biology, 15*(12), 550.

Nabavi, S. M., Šamec, D., Tomczyk, M., Milella, L., Russo, D., Habtemariam, S., et al. (2020). Flavonoid biosynthetic pathways in plants: Versatile targets for metabolic engineering. *Biotechnology Advances, 38*, Article 107316.

Naik, J., Misra, P., Trivedi, P. K., & Pandey, A. (2022). Molecular components associated with the regulation of flavonoid biosynthesis. *Plant Science, 317*, Article 111196.

Pertea, M., Pertea, G. M., Antonescu, C. M., Chang, T. C., Mendell, J. T., & Salzberg, S. L. (2015). StringTie enables improved reconstruction of a transcriptome from RNA-seq reads. *Nature Biotechnology, 33*(3), 290–295.

Qing, Z., Liu, J., Yi, X., Liu, X., Hu, G., Lao, J., et al. (2021). The chromosome-level *Hemerocallis citrina* Borani genome provides new insights into the rutin biosynthesis and the lack of colchicine. *Horticulture Research, 8*(1), 89.

Roy, A., Khan, A., Ahmad, I., Alghamdi, S., Rajab, B. S., Babalghith, A. O., et al. (2022). Flavonoids a bioactive compound from medicinal plants and its therapeutic applications. *BioMed Research International, 2022*, Article 5445291.

Sawai, S., & Saito, K. (2011). Triterpenoid biosynthesis and engineering in plants. *Frontiers in Plant Science, 2*, 25.

Shannon, P., Markiel, A., Ozier, O., Baliga, N. S., Wang, J. T., Ramage, D., et al. (2003). Cytoscape: A software environment for integrated models of biomolecular interaction networks. *Genome Research, 13*(11), 2498–2504.

Shen, N., Wang, T., Gan, Q., Liu, S., Wang, L., & Jin, B. (2022). Plant flavonoids: Classification, distribution, biosynthesis, and antioxidant activity. *Food Chemistry, 383*, Article 132531.

Skrajda-Brdak, M., Dąbrowski, G., & Konopka, I. (2020). Edible flowers, a source of valuable phytonutrients and their pro-healthy effects – a review. *Trends in Food Science and Technology, 103*, 179–199.

Tamura, K., Stecher, G., & Kumar, S. (2021). MEGA11: Molecular evolutionary genetics analysis version 11. *Molecular Biology and Evolution, 38*(7), 3022–3027.

Thapa, R., Afzal, O., Alfawaz Altamimi, A. S., Goyal, A., Almalki, W. H., Alzarea, S. I., et al. (2023). Galangin as an inflammatory response modulator: An updated overview and therapeutic potential. *Chemico-Biological Interactions, 378*, Article 110482.

Tovar, R., de Ceglia, M., Ubaldi, M., Rodríguez-Pozo, M., Soverchia, L., Cifani, C., et al. (2023). Administration of linoleoylethanolamide reduced weight gain, dyslipidemia, and inflammation associated with high-fat-diet-induced obesity. *Nutrients, 15*(20), 4448.

Wang, M., Carver, J. J., Phelan, V. V., Sanchez, L. M., Garg, N., Peng, Y., et al. (2016). Sharing and community curation of mass spectrometry data with global natural products social molecular networking. *Nature Biotechnology, 34*(8), 828–837.

Wang, N., Liu, W., Zhang, T., Jiang, S., Xu, H., Wang, Y., et al. (2018). Transcriptomic analysis of red-fleshed apples reveals the novel role of MdWRKY11 in flavonoid and anthocyanin biosynthesis. *Journal of Agricultural and Food Chemistry, 66*(27), 7076–7086.

Wickham, H. (2016). *ggplot2: Elegant graphics for data analysis. SpringerLink*. https://doi.org/10.1007/978-3-319-24277-4_5

Yang, C., Shen, S., Zhou, S., Li, Y., Mao, Y., Zhou, J., et al. (2022). Rice metabolic regulatory network spanning the entire life cycle. *Molecular Plant, 15*(2), 258–275.

Yang, H., Zhang, Y., Zhen, X., Guo, D., Guo, C., & Shu, Y. (2020). Transcriptome sequencing and expression profiling of genes involved in daylily (*Hemerocallis citrina* Borani) flower development. *Biotechnology and Biotechnological Equipment, 34*(1), 542–548.

Zhao, R., Luo, J., & Xu, B. (2024). Insights into secondary metabolites and health promoting effects of edible flower *Hemerocallis citrina* Baroni. *Journal of Functional Foods, 116*, Article 106133.